How μ-Opioid Receptor Recognizes Fentanyl

Quynh N. Vo,[†,‡] Paween Mahinthichaichan,[†,‡] Jana Shen,[*,‡] and Christopher R. Ellis[*,†]

† *Center for Drug Evaluation and Research, United State Food and Drug Administration, Silver Spring, Maryland 20993*

‡ *Department of Pharmaceutical Sciences, University of Maryland School of Pharmacy, Baltimore, Maryland 21201*

Received August 13, 2020; E-mail: Jana.Shen@rx.umaryland.edu; Christopher.Ross.Ellis@gmail.com

Abstract: The opioid crisis has escalated during the COVID-19 pandemic. More than half of the overdose-related deaths are related to synthetic opioids represented by fentanyl which is a potent agonist of mu-opioid receptor (mOR). In recent years, crystal structures of mOR complexed with morphine derivatives have been determined; however, structural basis of mOR activation by fentanyl-like synthetic opioids remains lacking. Exploiting the X-ray structure of mOR bound to a morphinan ligand and several state-of-the-art simulation techniques, including weighted ensemble and continuous constant pH molecular dynamics, we elucidated the detailed binding mechanism of fentanyl with mOR. Surprisingly, in addition to the orthosteric site common to morphinan opiates, fentanyl can move deeper and bind mOR through hydrogen bonding with a conserved histidine H297, which has been shown to modulate mOR's ligand affinity and pH dependence in mutagenesis experiments, but its precise role remains unclear. Intriguingly, the secondary binding mode is only accessible when H297 adopts a neutral HID tautomer. Alternative binding modes and involvement of tautomer states may represent general mechanisms in G protein-coupled receptor (GPCR)-ligand recognition. Our work provides a starting point for understanding mOR activation by fentanyl analogs that are emerging at a rapid pace and assisting the design of safer analgesics to combat the opioid crisis. Current protein simulation studies employ standard protonation and tautomer states; our work demonstrates the need to move beyond the practice to advance our understanding of protein-ligand recognition.

INTRODUCTION

The opioid crisis has escalated during the COVID-19 pandemic. Opioids are highly effective pain relievers, but their addictive nature can easily lead to abuse and overdose-related deaths. Overdose deaths from synthetic opioids, represented by fentanyl and its derivatives, are now associated with more deaths than any other type of opioids.[1] The surge in fentanyl is attributed to high potency (50–400 times more potent than the naturally occurring morphine), fast onset, straightforward synthesis, and low cost production.[2–5] Additionally, the fentanyl core is readily modified creating a vast chemical space of fentanyl analogs with abuse potential.[6]

Fentanyl and morphine opioids produce strong analgesic responses through binding and subsequent activation of a class A G protein-coupled receptor (GPCR) μ-opioid receptor (mOR).[7] In recent years, high-resolution crystal structures of mOR in complex with the morphinan agonist BU72,[8] antagonist β-FNA,[9] as well as the endogenous peptide analog agonist DAMGO[10] have been determined, featuring a salt bridge between a charged amine group of the ligand and a conserved residue Asp147 ($D^{3.32}$ in the Ballesteros-Weinstein numbering[11]) of mOR. The morphinan compounds and peptide analog also interact with a conserved His297 ($H^{6.52}$ in the Ballesteros-Weinstein numbering[11]) via water-mediated hydrogen bonds. Mutagenesis studies demonstrated that mutation of either Asp147 or His297 as well as a reduced pH (which presumably protonates His297) decreases the binding affinities for DAMGO and naloxone (antagonist).[12–14]

Despite the importance, surprisingly little is known about the signaling mechanism of fentanyl and how it interacts with mOR to illicit analgesic response.[5] It is conceivable that fentanyl and its analogs bind and activate mOR in the same manner as morphinan compounds; however, the structural basis remains lacking. The aforementioned mutagenesis experiments performed to probe the role of Asp147 and His297 were inconclusive due to excessive non-specific binding of fentanyl.[14] Docking[15,16] and long-time molecular dynamics (MD) simulations[17] based on the docked structure of fentanyl in mOR confirmed the stability of the orthosteric binding mode involving the salt bridge with Asp147; however, the role of His297 has not been explored.

Towards understanding the molecular mechanism of mOR activation by fentanyl, here we elucidate the detailed fentanyl-mOR binding mechanism by exploiting the morphinan-bound mOR crystal structure and several state-of-the-art molecular dynamics (MD) methods, including the weighted ensemble (WE) approach[18–20] for enhanced path sampling and continuous constant-pH MD (CpHMD) with replica-exchange[21–23] for pH titration of transmembrane proteins. Surprisingly, WE path sampling found that when His297 adopts the HID tautomer, fentanyl can move deeper into the mOR and establish an alternative binding mode through hydrogen bonding with His297. CpHMD titration showed that His297 favors the HIE tautomer in the apo mOR; however, interaction with the piperidine amine of fentanyl locks it in the HID tautomer. Additional microsecond equilibrium simulations were conducted to further verify the two binding modes and generate fentanyl-mOR interaction fingerprints. Alternative binding modes and involvement of tautomer states may represent general mechanisms in GPCR-ligand recognition. Our work provides a basis for understanding mOR activation by diverse fentanyl derivatives that are emerging on the dark market at a rapid pace. The molecular mechanism by which structural modifications alter fentanyl potency and abuse potential can inform the design of safer analgesics to combat the opioid crisis.

RESULTS AND DISCUSSION

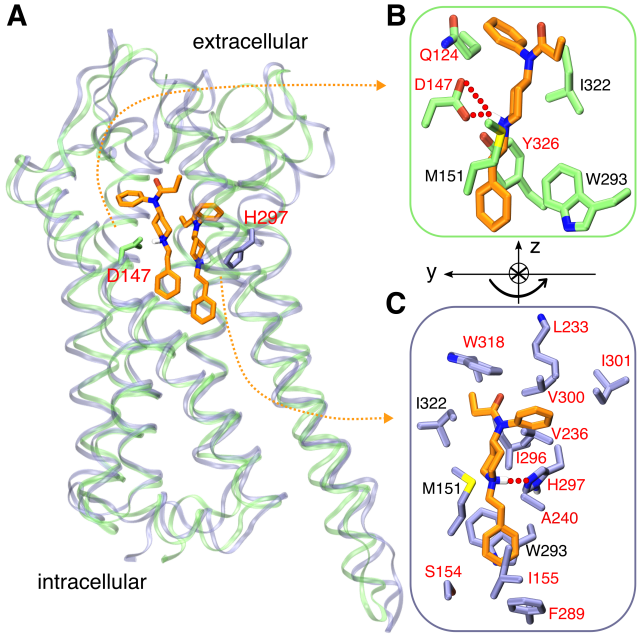

Figure 1. **Fentanyl binding with mOR. A.** Overlay of the representative simulation snapshots showing mOR is bound to fentanyl in the D147- (green) and H297- (purple) binding modes. **B.** Zoomed-in view of the D147-binding mode, in which the charged piperidine amine of fentanyl forms a salt bridge with Asp147. **C.** Zoomed-in view of the H297-binding mode, where the piperidine amine donates a proton to Nϵ of HID297. The curved arrow illustrates the change in the orientation of fentanyl in going from D147- to H297-binding mode. mOR residues making significant contacts with fentanyl (fraction greater than 0.5) are shown (see Fig. 4). Those unique to the two binding modes are labeled in red and otherwise in black.

Table 1. Simulation summary.

Name	Type	Starting Configuration		Time
		Binding Mode	H297 State	(μs)
WE-HIE	WE	D147 salt bridge	HIE	24.3
WE-HID	WE	D147 salt bridge	HID	23.6
CpH-apo	CpHMD	apo active mOR	Dynamic	0.32
CpH-D147	CpHMD	D147 salt bridge	Dynamic	0.32
CpH-H297	CpHMD	H297 hydrogen bond	Dynamic	0.32
MD-D147(HID)	equil. MD	D147 salt bridge	HID	0.5
MD-D147(HIE)	equil. MD	D147 salt bridge	HIE	0.5
MD-D147(HIP)	equil. MD	D147 salt bridge	HIP	0.5
MD-H297(HID)	equil. MD	H297 hydrogen bond	HID	1.0
MD-H297(HIE)	equil. MD	H297 hydrogen bond	HIE	1.0
MD-H297(HIP)	equil. MD	H297 hydrogen bond	HIP	1.0

Fentanyl unbinds from the D147-bound configurations in the presence of HIE297. Following the 115-ns MD to relax the docked fentanyl-mOR complex (details see Methods and Protocols and Fig. S1), we performed WE all-atom MD simulations to explore the detailed binding interactions of fentanyl in mOR. The fentanyl RMSD was used as the progress coordinate. The MD trajectories were produced using the GPU-accelerated PMEMD engine in AMBER18[24] and the Python-based WESTPA tool[19] was used to control the WE protocol.

In the first WE simulation of 24 μs aggregate time, His297 was fixed in the HIE tautomer (Nϵ atom of imidazole is protonated), as in the recent mOR simulations by the Dror goup.[8,10] The WE-HIE simulation proceeded as expected. In the first 75 iterations or 2.5 μs of cumulative sampling time, fentanyl's piperidine stays near Asp147, sampling both the salt-bridged and solvent-separated configurations, with the FEN–D147 distance (minimum heavy-atom distance between the piperidine amine and the carboxylate) below 5 Å (Fig. 2A and Fig. S2B). During this time, fentanyl ΔZ (center of mass Z position relative to mOR) fluctuates between 7.5 and 10.5 Å (Fig. S2D), and RMSD stays below 4 Å (Fig. S2A). After 75 iterations, fentanyl starts to move upward and away from Asp147; after about 140 iterations or 8 μs of cumulative sampling time, RMSD increases to above 7.5 Å and ΔZ starts to sample values above 14 Å, indicating that fentanyl is on the way to exit mOR (Fig. S2A-C). At the end of 300 iterations or 24 μs of cumulative sampling time, fentanyl reaches the extracellular end of mOR (Fig. S2D). It is noteworthy that in the WE-HIE simulation, the FEN–H297 distance from the piperidine nitrogen to the unprotonated imidazole nitrogen is always above 4 Å, indicating that fentanyl's piperidine does not form hydrogen bond interactions with His297 (Fig. 2A and Fig. S2C). Interestingly, even with the intact piperidine–D147 salt bridge, fentanyl can sample various configurations with a RMSD as high as 8 Å (Fig. S2A,B).

Fentanyl samples both D147- and H297-bound configurations in the presence of HID297. In addition to HIE, a neutral histidine can adopt the HID tautomer state, whereby the Nδ atom is protonated. Considering the important and yet unclear role of His297 in opioid-mOR binding, we conducted another WE simulation with His297 fixed in HID (WE-HID). Surprisingly, fentanyl did not exit mOR as was observed in the WE-HIE simulation. After about 27 iterations or 0.6 μs of cumulative sampling time, some of the trajectories start to sample configurations in which fentanyl laterally rotates 120°, translates 2 Å, and moves down 1 Å, enabling the formation of a stable hydrogen bond between the piperidine amine and the unprotonated Nϵ atom of HID297, (Fig. 1A, Fig. 2B, and Fig. S3). At the same time, the RMSD remains below 7 Å. Unexpectedly, after about 210 iterations or 13 μs of cumulative sampling time, some trajectories start to sample configurations in which fentanyl is inserted deeper into the receptor (Fig. S3D). At the end of 20 μs aggregate time, fentanyl continues to sample the D147- and HID297-bound configurations along with positions in which it does not interact with either residues (Fig. 2B and Fig. S3); however, the fentanyl ΔZ stay below 14 Å, indicating that it remains inside of the ligand accessible vestibule of mOR (Fig. 2B and Fig. S3D).

Further comparison between the configurations from the WE-HIE and WE-HID simulations. To further understand the differences in the configuration space sampled by fentanyl in the presence of HIE297 and HID297, we plotted FEN–H297 vs. FEN–D147 distance and color coded the data points by ΔZ of fentanyl. Corroborating with the previous analysis, these plots show that while the D147-bound configurations (FEN–D147 distance $\leq$ 3.5 Å) are sampled in both WE-HIE and WE-HID simulations, the H297-bound configurations (FEN–H297 distance $\leq$ 3.5 Å) are only sampled in the WE-HID simulation (Fig. 2C and D). Further, the H297-bound configurations sample lower ΔZ positions of 3–8 Å, as compared to the D147-bound configurations whereby ΔZ is in the range of 7–13 Å, (Fig. 2C-F, and Fig. S3, S4). Interestingly, the WE-HID simulation also sampled fentanyl configurations deeply embedded in mOR (ΔZ $\leq$ 3 Å) but without a hydrogen bond with HID297 (FEN–H297 distance of 4–6 Å), suggesting that the piperidine–HID297 hydrogen bond may not be the only stabilizing factor for the deep insertion of fentanyl in mOR (Fig. 2D and Fig. S4). Representative snapshots sug-

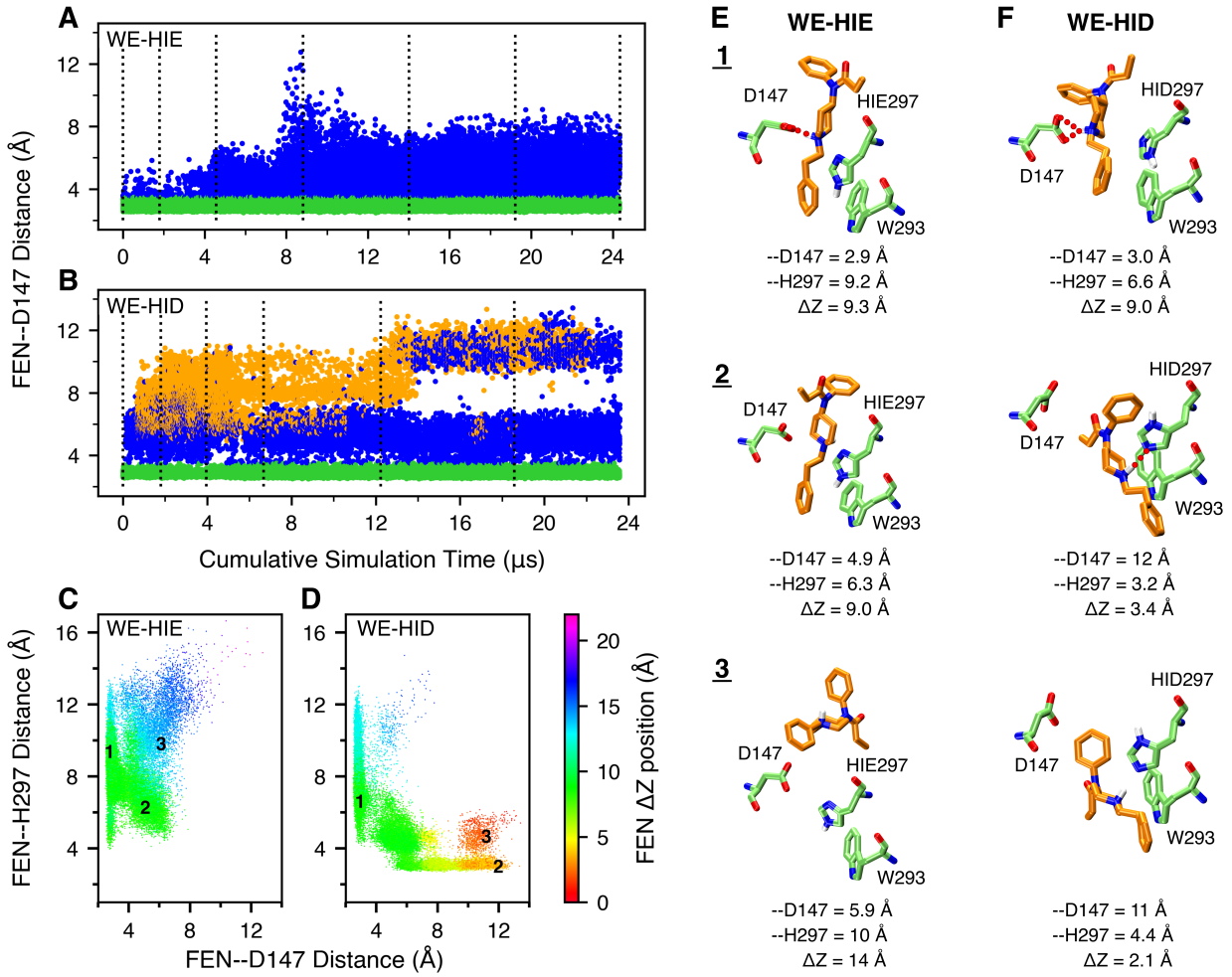

Figure 2. **Fentanyl visits the D147-binding mode in the presence of HIE297 but both D147- and H297-binding modes in the presence of HID297. A, B.** The FEN–D147 distance, referred to as the minimum distance between the piperidine nitrogen and the carboxylate oxygen of Asp147, as a function of the cumulative WE simulation time in the presence of HIE297 (A) or HID297 (B). Data with the FEN–D147 and FEN–H297 distances below 3.5 Å are colored green and orange, respectively, and otherwise blue. The unweighted data from all bins were taken and the time refers to the cumulative time. The dotted vertical lines are drawn at every 50 WE iterations. **C, D.** FEN–H297 vs. FEN–D147 distance from the WE-HIE (C) and WE-HID (D) simulations. The data points are color coded by the fentanyl ΔZ position, defined as the distance between the centers of mass (COM) of fentanyl and mOR in the z direction. N- (52–65) and C-terminal (336–347) residues of mOR were excluded from the COM calculation. The FEN–H297 distance is measured between the piperidine nitrogen and the unprotonated imidazole nitrogen of His297. Three groups of data (labeled in the plots) taken from the last 50 iterations of each simulation were subjected to the hierarchical clustering analysis. For WE-HIE, the three groups were defined as FEN–D147 distance $\leq$ 3.5 Å; FEN–D147 distance $\geq$ 4 Å and FEN–H297 distance $\leq$ 8 Å; and FEN–D147 distance $\geq$ 4 Å and FEN–H297 distance $\geq$ 8 Å. For WE-HID, the three groups were defined as FEN–D147 distance $\leq$ 3.5 Å; FEN–H297 distance $\leq$ 3.5 Å; and FEN–D147 distance $\geq$ 8.5 Å and FEN–H297 distance $\geq$ 4 Å. **E, F.** Representative structures of the most populated clusters from the WE-HIE (E) and WE-HID (F) data defined in C and D. The FEN–D147 and FEN–H297 distances and the fentanyl ΔZ position are given.

gest that the interactions between the phenylethyl group and Trp293 may be a contributor (Fig. 2F). Note, the WE simulations are likely not converged and a quantitative description of the thermodynamics and kinetics of fentanyl dissociation is beyond the scope of the current work.

His297 favors the HIE tautomer in the apo mOR but the piperidine–HID297 interaction locks His297 in the HID state. The WE simulations suggest that fentanyl has an alternative binding mode which may be promoted by the presence of the HID tautomer of His297. To determine the physiological relevance, we carried out titration simulations using the membrane-enabled hybrid-solvent CpHMD method with pH replica exchange[21,22] to determine the protonation state of His297 under physiological pH for the apo mOR and the fentanyl-bound mOR in the D147- and the H297 binding modes. For each system, 16 pH replicas were simulated in the pH range 2.5–9.5, with the aggregate sampling time of 320 ns. The calculated pK_a of His297 is well converged (Fig. S4).

In the absence of ligand (CpH-apo simulation), the calculated macroscopic pK_a of His297 is 6.8. At physiological pH 7.4, the HIE tautomer is predominantly sampled at 64%, while the HID tautomer and the charged HIP populations are 12% and 24%, respectively (Fig. 3A). The presence of fentanyl in the D147-binding mode upshifts the His297 pK_a to 7.3 (CpH-D147 simulation). At physiological pH, both HIE and HIP are the predominant forms accounting for 39% and 44% of the population, respectively, while HID accounts for 17% of the population (Fig. 3B). Finally, CpHMD titration was performed for the fentanyl-mOR complex in the H297-binding

mode (CpH-H297 simulation). Interestingly, the calculated pK_a is 6.7, nearly the same as for the apo mOR; however, at physiological pH HID is the predominant form with a population of 60%, while the HIE and HIP forms account for 20% each. Importantly, the protonation state of His297 is coupled to its distance to the piperidine amine of fentanyl (Fig. 3D). When the piperidine nitrogen is within 4 Å of the Nϵ atom of His297, the HID state is exclusively sampled, whereas the HIE and HIP states are only allowed when the piperidine–His297 distance is $\geq$ 7 Å (Fig. 3D). Together, the CpHMD data demonstrate that ligand interaction perturbs the protonation state of His297: while the apo mOR preferably samples HIE297, the population of HIP or HID state may increase upon ligand binding. When fentanyl interacts with Asp147, the HIP state is sampled with an equal probability as HIE, and when fentanyl interacts with His297, HID is the preferred state. These data provide an explanation as to why the H297-binding mode (quickly) emerged in the WE simulation with HID297 but not HIE297.

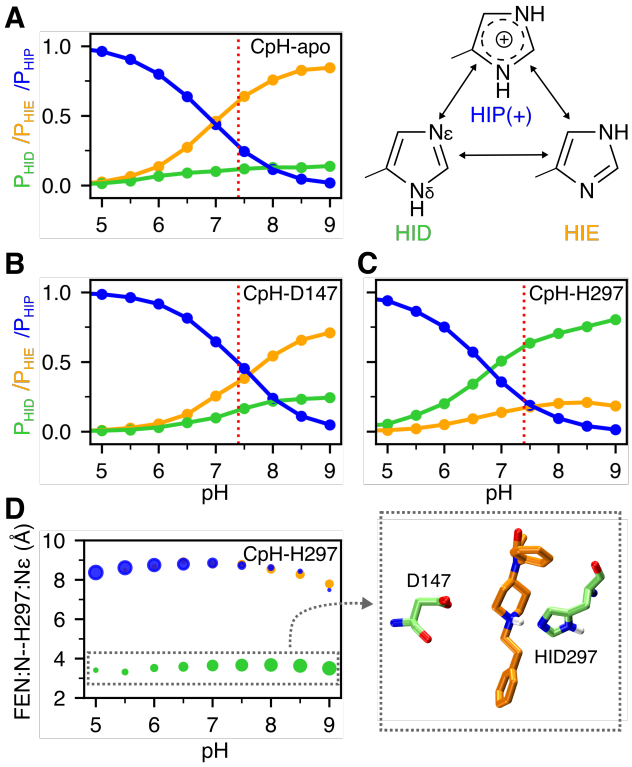

Figure 3. **Protonation state of His297 is influenced by fentanyl binding. A, B, C.** Occupancies of the HID (green), HIE (orange), and HIP (blue) states of His297 as a function of pH from the replica-exchange CpHMD simulations of the apo mOR (**A**) and fentanyl-bound complex in the D147- (**B**) and H297-binding mode (**C**). The three states are in equilibrium through protonation/deprotonation and tautomerization. **D.** Average distance between the piperidine nitrogen and His297's Nϵ at different pH conditions when His297 is in the HID (green), HIE (orange), or HIP (blue) state. The area of the data point is proportional to the occupancy of the protonation state. A zoomed-in snapshot corresponding to the HID state is shown.

The D147-binding mode is stable regardless of the protonation state of H297. To further characterize fentanyl-mOR interactions and delineate the impact of the His297 protonation state, we carried out a series of equilibrium simulations. First, three 0.5-μs simulations were initiated from the equilibrated fentanyl-mOR complex in the D147-binding mode with His297 fixed in the HID, HIE, and HIP states (Table 1). To quantify ligand-receptor interactions, the fractions of time for the mOR residues that form at least one heavy atom contact with fentanyl were calculated (Fig. 4A-D, top panels). To determine what parts of fentanyl contribute to the receptor recognition, a fingerprint matrix was calculated which shows the contacts formed between specific mOR residues and fentanyl substituents (Fig. 4A-D, bottom panels). Simulations starting from the D147-binding mode demonstrated that many interactions are independent of the protonation state of His297. Most importantly, the piperidine–D147 salt bridge remains stable throughout the 0.5-μs trajectories with HIE297, HID297, and HIP297 (Fig. S5 and red bars in Fig. 4A-C), consistent with the WE simulations. Interestingly, while maintaining the salt bridge with piperidine, Asp147 also interacts with phenyl and phenethyl at the same time (Figure 4A-C, bottom panels), which may provide further stabilization to the D147-binding mode.

Another important fentanyl-mOR contact is the aromatic stacking interaction between the phenyl ring of the phenethyl group and Trp293 (Fig. 1B, Fig. 4A-C bottom panels, and Fig. S6), which remains stable in all three simulations. The importance of the phenethyl group at this location in the 4-anilidopiperidine core of fentanyl is supported by the observations that substitution with methyl (as in N-methyl-fentanyl) increases the K_i value by about 40 fold,[25] and removal of one ethylene group renders the ligand inactive.[26] However, substitution with a different aromatic ring, e.g thiophene in sufentanil and ethyl tetrazolone in alfentanil, does not appear to be have a significant effect on binding affinity, although the latter ligands have an O-methyl group at the 4-axial hydrogen position.[3]

Fentanyl-mOR interaction profiles vary with different protonation state of His297 albeit in the same D147-binding mode. Despite the similarities, the fentanyl-mOR interaction profiles obtained from the simulations MD-D147(HID), MD-D147(HIE), MD-D147(HIP) show differences (Fig. 4A-C). To quantify the overall difference between two interaction profiles, the Tanimoto coefficient (T_c)[27] was calculated (Fig. 5A), where T_c of 1 indicates that identical mOR residues are involved in binding to fentanyl. Accordingly, the contact profiles with HIE297 and HIP297 are more similar (T_c of 0.81), whereas the contact profiles with HID297 and HIE297/HIP297 are somewhat less similar (T_c of 0.71/0.73). As to the latter, the most significant differences are in the N-terminus. While fentanyl makes no contact with the N-terminus in the simulation with HID297, it interacts via propanamide and phenyl groups with His54 and Ser55 in the simulations with HIE297/HIP297. The fentanyl–N-terminus interactions are consistent with an experimental study which demonstrated that truncation of the mOR N-terminus increases the dissociation constant of fentanyl by 30 fold.[28] Significant differences are also seen in the TM2 contacts between simulations with HIE297 and HID297/HIP297. Four TM2 residues, Ala113, Asp114, Ala117, Gln124, are involved in stable interactions with fentanyl in the simulations with HID297/HIP297; however, only one TM2 residue Gln124 contacts fentanyl in the simulation with HIE297 (Fig. 4A-C, top panels). A closer examination revealed that Gln124 interacts with phenyl in the simulation with HID297/HIP297 but it additionally interacts with propanamide in the simulation with HIE297, forming a stable hydrogen bond (Fig. 4A and B, bottom panels, Fig. S7A and B). This hydrogen bond

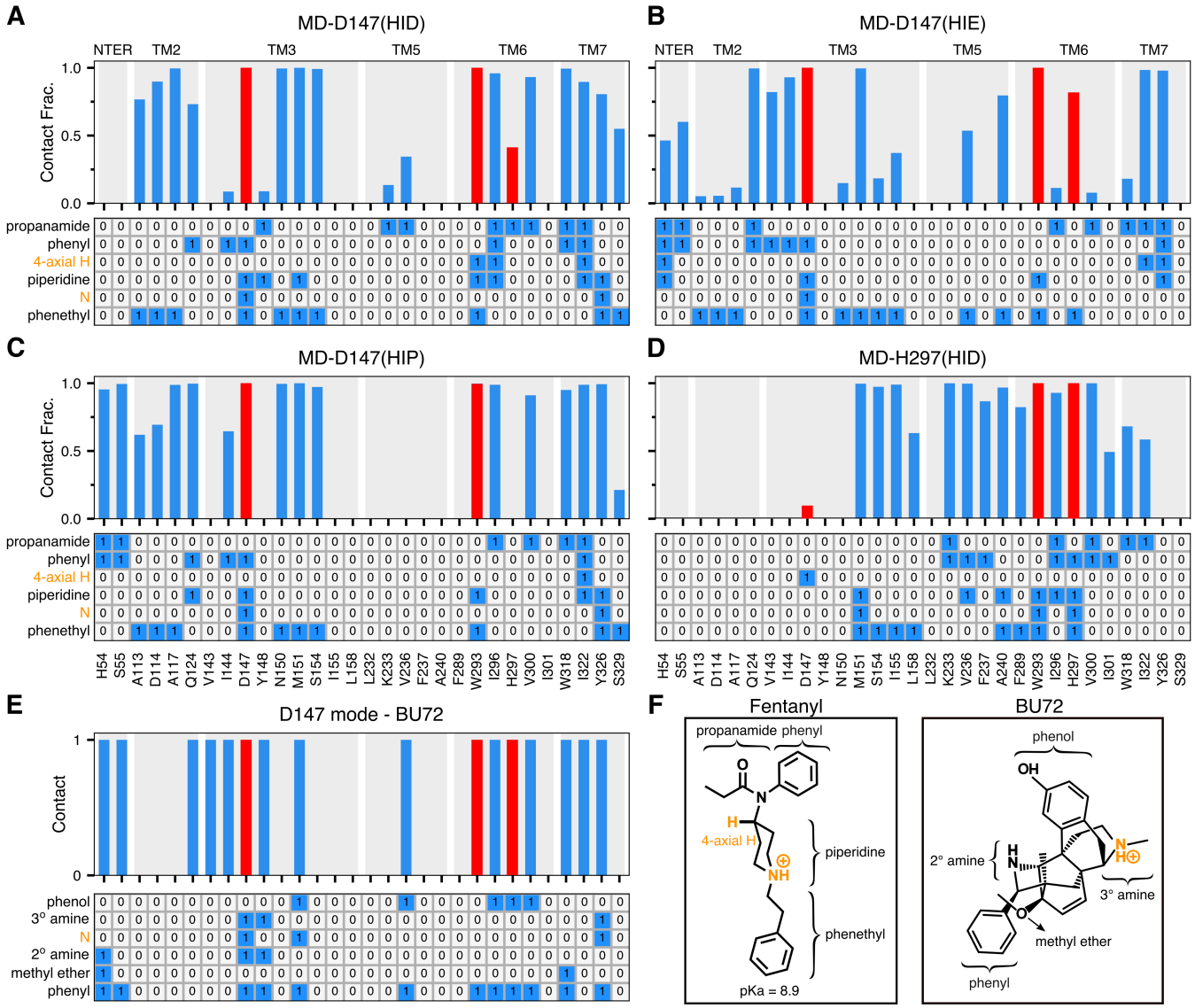

Figure 4. **Fentanyl-mOR interaction profiles in the presence of different protonation state of His297 and comparison to the BU72-mOR contacts in the crystal structure. A-D Top.** Fraction of time that mOR residues form contacts with fentanyl in the equilibrium MD starting from the D147- (**A, B, C**) and H297-binding modes (**D**). A contact is considered formed if any sidechain heavy atom is within 4.5 Å of any fentanyl heavy atom. Only residues that form contacts for least 25% of the time in at least one of the six equilibrium simulations are shown. Contacts with Asp147, Trp293, and His297 are highlighted in red. **A-D Bottom.** Ligand-mOR fingerprint matrix showing the fentanyl groups as rows and mOR residue as columns. 1 represents in contact and 0 represents no contact. **E.** mOR residues forming contacts with BU72 in the crystal structure (PDB: 5C1M[8]). **F.** Chemical structure of fentanyl and BU72. Different substituent groups are labeled. The 4-axial hydrogen and amine nitrogen of the piperidine group are indicated.

may contribute to an upward shift of fentanyl's position in the simulation with HIE297 (see later discussion), resulting in a decrease of the aromatic stacking interaction between the phenyl ring of the phenethyl group and Trp293 (Fig. S6D).

The H297-binding mode is stabilized by many fentanyl-mOR contacts in the presence of HID297. To further evaluate the fentanyl-mOR interactions in the H297-binding mode, three 1-μs equilibrium simulations were initiated from the H297-binding mode with His297 fixed in the HID, HIE, and HIP states. We refer to these simulations as MD-H297(HID), MD-H297(HIE) and MD-H297(HIP), respectively (Table 1). In the MD-H297(HID) simulation, the piperidine–H297 hydrogen bond remains stable; however, the hydrogen bond immediately breaks and the N-Nϵ distance fluctuates around 7.5 Å and 8.0 Å in the simulations with HIE297 and HIP297, respectively (Fig. S8). These results are in agreement with the replica-exchange CpHMD titration, confirming that the H297-binding mode is only stable in the presence of HID297. In addition to the piperidine–H297 hydrogen bond, the simulation MD-H297(HID) shows that fentanyl forms stable contacts with over a dozen of residues on TM3, TM5, TM6, and TM7 (Fig. 1C and Fig. 4D), which explains the remarkable stability of the H297-binding mode in both MD-H297(HID) and WE-HID simulations.

Comparison of the fentanyl-mOR contact profiles in the two binding modes. Several interactions, e.g., stable contacts with Met151 (TM3), Trp293 (TM6), and Ile322 (TM7), are shared among all equilibrium simulations, regardless of the binding mode or His297 protonation state (Fig. 1B and C, Fig. 4A-D). Among them is the aromatic stacking between

the phenethyl group and Trp293 (Fig. 4A-D, Fig. S6), which is stable in all simulations. Nonetheless, the contact profile from the simulation MD-H297(HID) is drastically different from those in the D147-binding mode. The T_c value comparing MD-H297(HID) with MD-D147(HID), MD-D147(HIE), and MD-D147(HIP) are 0.44, 0.46 and 0.31, respectively (Fig. 5A). Fentanyl contacts with the N terminus and TM2 residues are completely absent and fewer TM7 residues are involved in fentanyl interactions in the simulation MD-H297(HID) (Fig. 4D). As His297 is slightly below Asp147, a switch from the piperidine–D147 salt bridge to the piperidine–H297 hydrogen bond results in a lower vertical position for fentanyl as compared to the D147-binding mode. The change in the vertical position likely contributes to the differences in the mOR residues interacting with fentanyl.

The fentanyl–H297 interactions also appear to perturb the local environment. While the backbone amide–carbonyl hydrogen bond between His297 and Trp293 is present in all equilibrium simulations, the backbone carbonyl of Trp293 also accepts a stable hydrogen bond from the Nδ atom of HID297 in the simulation MD-H297(HID) (Fig. S7A and C). We hypothesize that the hydrogen-bond network (fentanyl–HID297–Trp293) together with the aromatic stacking between the phenethyl group and Trp293 contributes to a slight increase in the χ_2 angle of Trp293 (125±9.0°), as compared to that in the D147-binding mode simulations (112±10° with HIE297, 116±9.6° with HID297, and 110±9.5° with HIP297). Interestingly, the χ_2 angle of Trp293 in the X-ray structure of active mOR bound to BU72 (PDB: 5C1M[8]) is 120°, while that in the X-ray structure of the inactive mOR bound to the antagonist β-FNA (PDB: 4DKL[9]) is 80°.

Another intriguing feature of the simulation MD-H297(HID) is the transient contact between Asp147 and the 4-axial hydrogen of the piperidine ring (Fig. 4D and F). In the simulations of the D147-binding mode, the 4-axial hydrogen makes contact with TM6 or TM7 residues (Fig. 4A–C); however, in the simulation of the H297-binding mode, since the piperidine position is lower due to hydrogen bonding with His297, the 4-axial hydrogen position is also lowered, enabling an interaction with Asp147. Thus, we hypothesize that a substitution for a larger polar group at the 4-axial position might add stable interactions to both the D147- and H297-binding modes, which would potentially explain the increased binding affinity of fentanyl analogs with a methyl ester substitution at the 4-axial position, e.g. carfentanil and remifentanil.[2,25,29]

Comparison of the position and conformation of fentanyl in different binding modes. The WE simulations demonstrated that the two fentanyl binding modes are readily accessible from one another in the presence of HID297 (Fig. 2D). The equilibrium simulations found that fentanyl contacts His297 in the D147-binding mode with HID297 or HIE297 (Fig. 4A and B) and it transiently interacts with Asp147 in the H297-binding mode with HID297 (Fig. 4D). To quantify the spatial relationship between the two binding modes, we calculated the center of mass (COM) positions of fentanyl and key contact residues relative to that of mOR based on the equilibrium simulations of the D147- and H297-binding modes and plotted in the (Y,Z) and (X,Y) planes. The resulting side (Fig. 5B) and top (Fig. 5C) views of the fentanyl and mOR residue locations showed that fentanyl adopts a similar position in the simulations of the D147-binding mode with HIE297 or HIP297; however, intriguingly, with HID297, the fentanyl position is moved towards the position it takes in the simulation of the H297-binding mode. Specifically, in going from the D147- to the H297-binding mode, fentanyl laterally rotates by about 120° such that the piperidine amine faces the Nϵ atom of His297, and translates by about 2 Å on the (X,Y) plane before moving down the Z axis (Fig. 5B and C). The simulation MD-H297(HID) gave the fentanyl ΔZ of 7.4±0.4 Å, as compared to 8.3±0.4, 8.8±0.3, and 9.2±0.5 from the simulations MD-D147(HID), MD-D147(HID), and MD-D147(HIP), respectively. Additionally, fentanyl is in a more upright position in the simulation of the H297 binding mode, with a vertical angle of 15°, compared to the angle of 20–40° in the simulations of the D147 binding mode (Fig. S10).

A closer look at the conformation of His297 suggests that its χ_2 dihedral angle may be modulated by the protonation/tautomer state (Fig. S11). When His297 is in the HIE or HIP state, only the negative χ_2 angle is sampled regardless of the binding mode; however, in the presence of HID297, the simulation of the D147-binding mode samples both negative and positive χ_2 angles, whereas the simulation of the H297-binding mode only samples the positive χ_2 angle. Thus, it is possible that HID297 allows both rotameric states, while

A

	MD-D147 (HID)	MD-D147 (HIE)	MD-D147 (HIP)	MD-H297 (HID)	D147 mode - BU72
MD-D147 (HID)	1				
MD-D147 (HIE)	0.71	1			
MD-D147 (HIP)	0.73	0.81	1		
MD-H297 (HID)	0.44	0.46	0.31	1	
D147 mode - BU72	0.57	0.71	0.57	0.38	1

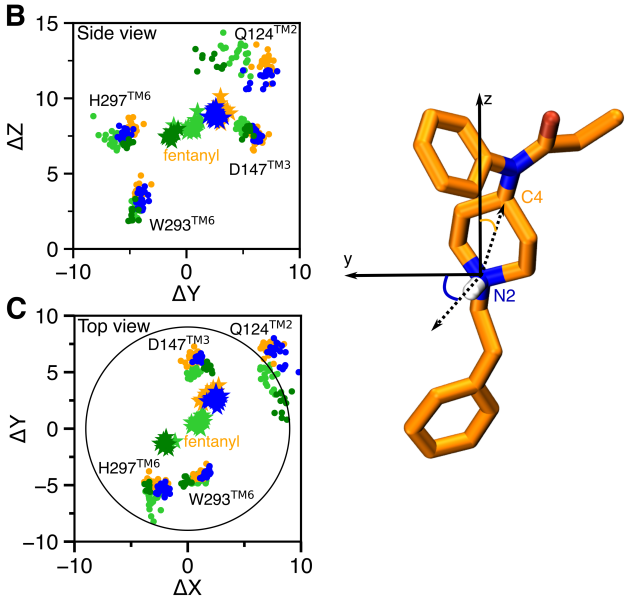

Figure 5. **Contact similarity and spatial relationship between the D147- and H297-binding modes. A.** Tanimoto coefficients (T_c) calculated using the binary contacts (details see Methods and Protocols). T_c ranges from 0 to 1, where 1 indicates identical mOR residues are involved in fentanyl binding in both simulations. **B, C.** Locations of fentanyl (stars) and critical amino acids (circles) plotted on the (Y,Z) and (X,Y) planes. A data points are sampled every 10 ns. The center of mass of mOR is set to origin. The data from MD-D147(HID), MD-D147(HIE), and MD-D147(HIP) are colored light green, orange, and blue, respectively, while the data from MD-H297(HID) are colored dark green. The z axis is the membrane normal, while the x axis is defined by the N2–H vector.

the piperidine–H297 hydrogen bond locks the angle at 100°. This data further supports the notion that the two binding modes are made accessible to one another in the presence of HID297.

Comparison to the X-ray structure of BU72-mOR complex. Finally, we compare the two fentanyl binding modes to the crystal structure of the BU72-bound mOR. The BU72-mOR binding profile is most similar to fentanyl's D147-binding profile in the presence of HIE297 (T_c of 0.71) due to their nearly identical interactions with the N-terminus, TM2 and TM3 and TM7. To a less extent, the BU72 binding profile shares similarities with the D147-binding profile with HID297 or HIP297 (T_c of 0.57 for both). Importantly, the six residues, Gln124 (TM2), Asp147 and Met151 (TM3), Trp293 (TM6), Ile322 and Tyr326 (TM7), which form the foundation of the D147 binding pocket for fentanyl (with contact fraction greater than 0.5 regardless of the protonation state of His297) are present in the BU72-mOR binding contacts (Fig. 4A-C). In contrast, the D147-BU72 contact profile has a much lower overlap with the H297-binding profile (T_c of 0.38).

CONCLUDING DISCUSSION

In summary, a set of state-of-the-art molecular dynamics simulations have been applied to investigate fentanyl binding to mOR. The WE simulations confirmed that fentanyl binds to mOR via the salt-bridge interaction between the piperidine amine and the conserved Asp147, consistent with the X-ray crystal structures of mOR in complex with BU72, β-FNA, and DAMGO.[8–10] However, surprisingly, when His297 is protonated at δ nitrogen (HID), fentanyl can also adopt a H297-binding mode, which features a hydrogen bond between the piperidine amine and the unprotonated ϵ nitrogen of HID297. The conventional single trajectory simulations confirmed that the D147-binding mode is stable regardless of the protonation state of His297, whereas the H297-binding mode is only compatible with HID297. The CpHMD titration revealed that in the absence of the piperidine amine–imidazole interaction, His297 can titrate via either Nδ or Nϵ; however, in the presence of the interaction, Nϵ loses the ability to gain a proton, locking histidine in the HID form.

It is important to consider the physiological relevance of the H297-binding mode. Mutations of His297 and a reduction in pH have been shown to decrease ligand affinity of mOR and modulate pH dependence in a number of experimental studies.[12–14] However, the experiments were inconclusive when performed with fentanyl.[14] Our data provides a piece of evidence that may explain the role of His297 in modulating fentanyl binding with the μ-opioid receptor. According to the CpHMD titration, at physiological pH, HIE297 is the predominant form in the apo mOR, and HID297 is least populated in both the apo and holo mOR in the D147-binding mode. Consistent with this data, the crystal structure based BU72-mOR contact profile bears the strongest resemblance to the simulated D147-binding mode with HIE297 as compared to HID297 or HIP297. Thus, we hypothesize that fentanyl primarily binds to mOR via the D147 mode under the physiological pH, while the H297-binding mode is a secondary state.

The X-ray structures of mOR in complex with BU72, β-FNA, and DAMGO[8–10] feature a water-mediated hydrogen bond between His297 and a phenol group in the ligand. In addition to the lack of a phenol group, fentanyl differs from morphinan structures in several other ways. Fentanyl has a more elongated shape; it is highly flexible with at least seven rotational bonds; and it has only two structural elements capable of forming hydrogen bonds (amine and carbonyl groups). In contrast, morphinan ligands are often rigid and possess more structural elements with hydrogen bonding capabilities. Therefore, it is possible that the H297-binding mode is unique to fentanyl and perhaps also its analogs but not morphinan ligands. Intriguingly, a combined MD and experimental study found that unlike synthetic antagonists, the endogenous agonist acetylcholine can diffuse into a much deeper binding pocket of M3 and M4 muscarinic acetylcholine receptors.[30] Thus, alternative binding modes may be a general phenomenon of GPCR-ligand recognition.

His297 has been discussed as an important residue that directly or indirectly contacts mOR in the D147-binding mode by previous MD studies conducted with the HIE or HID tautomer. Dror and coworkers confirmed that His297 (HIE) forms water-mediated interactions with BU72 and DAMGO as shown in the crystal structures.[8,10] Simulations of Carloni and workers[31] found that morphine and hydromorphone form direct and water-mediated hydrogen bonds with His297 (HID), respectively. Morphine was also shown to form stable hydrophobic interactions with His297 (protonation state unclear) in a recent MD study.[17] The de novo binding simulations of the Filizola group showed that oliceridine (TRV-130) which has an atypical chemical scaffold binds mOR via water-mediated interactions between the charged amine group and Asp147, while frequently contacting His297 (protonation state unclear).[32] While consistent with these studies, our data uncovered an unexpected role of the tautomer state in modulating the fentanyl-binding mechanism.

CpHMD titration allowed us to determine the protonation states of His297 and all other titratable sites, including the highly conserved residue Asp114 ($D^{2.50}$ in the Ballesteros-Wenstein numbering[11]). Both experiments[33] and simulations[8,10,34] demonstrated that $D^{2.50}$ is involved in binding a sodium ion in the inactive but not active state of GPCRs. Ion binding stabilizes the deprotonated Asp114 in the inactive mOR; however, the protonation state of Asp114 in the active mOR remains unclear. Considering the lack of sodium presence in the active mOR, two previous MD studies used a protonated Asp114,[8,10] while published work did not specify the protonation state.[17,31,32] Recently, the pK_a of $D^{2.50}$ in M2 muscarinic acetylcholine receptor (m2R) was calculated using the Poisson-Boltzmann method with a protein electric constant of 4.[35] The calculation gave a pK_a of 8–12 when sodium is 5 Å away from $D^{2.50}$. However, it is widely known that the continuum-based Poisson-Boltzmann methods overestimate the pK_a's of internal residues, particularly with a low dielectric constant (e.g., 4).[36] The CpHMD titration gave a pK_a of 4.8$\pm$0.30 in the apo active mOR and 5.1$\pm$0.26/0.29 in the fentanyl-bound forms in the D147- or H297-binding mode. Thus, the pK_a of $D^{2.50}$ is indeed upshifted relative to the solution or model value (3.8[37]), but it remains deprotonated at physiological pH.

Having a solution pK_a of 6.5[37] and two neutral tautomer forms, histidine may sample all three protonation states in the protein environment at physiological pH 7.4. Our work demonstrates that the tautomer state of histidine in the ligand access region may alter the mechanism and possibly also the thermodynamics and kinetics of ligand binding. Thus, the conventional treatment in MD simulations, i.e., fixing histidine in a neutral tautomer state following the program default (HIE

in Amber[24] and HID in CHARMM[38]) may not be appropriate for detailed investigations.

By combining CpHMD titration to determine protonation states and fixed-charge simulations for long-time-scale conformational sampling, our work led to new and surprising findings; however, a major caveat of the study is that all other histidines have been fixed in one protonation state in the WE and equilibrium simulations, even though some of them may sample alternative protonation state at physiological pH according to the CpHMD titration. A more complete understanding of how protonation states impact the conformational dynamics and ligand binding of GPCRs awaits the development of GPU-accelerated hybrid-solvent[21,22] and all-atom CpHMD methods[39] and their integration with enhanced sampling protocols such as the WE approach.[18,20,40] Notwithstanding the caveat, our work provides a starting point for understanding mOR activation by synthetic opioids and the molecular mechanisms by which structural modifications alter potency and abuse potential of fentanyl derivatives that are emerging at a rapid pace. A molecular understanding of mOR activation by synthetic ligands can also assist the design of safer analgesics to combat the opioid crisis.

Supporting Information Available

Supporting Information contains Methods and Protocol, Supplemental Tables, and Supplemental Figures.

Acknowledgement Q.N.V. is supported by an ORISE fellowship from the Department of Energy. Financial support from the National Institutes of Health (GM09888) to J.S. and P.M. is acknowledged.

References

(1) Synthetic Opioid Overdose Data | Drug Overdose | CDC Injury Center. https://www.cdc.gov/drugoverdose/data/fentanyl.html, 2020.
(2) Van Bever, W. F.; Niemegeers, C. J.; Schellekens, K. H.; Janssen, P. A. N-4-Substituted 1-(2-Arylethyl)-4-Piperidinyl-N-Phenylpropanamides, a Novel Series of Extremely Potent Analgesics with Unusually High Safety Margin. *Arzneimittelforschung.* **1976**, *26*, 1548–1551.
(3) Volpe, D. A.; Tobin, G. A. M.; Mellon, R. D.; Katki, A. G.; Parker, R. J.; Colatsky, T.; Kropp, T. J.; Verbois, S. L. Uniform Assessment and Ranking of Opioid Mu Receptor Binding Constants for Selected Opioid Drugs. *Regul. Toxicol. Pharmacol.* **2011**, *59*, 385–390.
(4) Burns, S. M.; Cunningham, C. W.; Mercer, S. L. DARK Classics in Chemical Neuroscience: Fentanyl. *ACS Chem. Neurosci.* **2018**, *9*, 2428–2437.
(5) Comer, S. D.; Cahill, C. M. Fentanyl: Receptor Pharmacology, Abuse Potential, and Implications for Treatment. *Neurosci. Biobehav. Rev.* **2019**, *106*, 49–57.
(6) Vardanyan, R. S.; Hruby, V. J. Fentanyl-Related Compounds and Derivatives: Current Status and Future Prospects for Pharmaceutical Applications. *Future Med. Chem.* **2014**, *6*, 385–412.
(7) Pathan, H.; Williams, J. Basic Opioid Pharmacology: An Update. *Br. J. Pain* **2012**, *6*, 11–16.
(8) Huang, W.; Manglik, A.; Venkatakrishnan, A. J.; Laeremans, T.; Feinberg, E. N.; Sanborn, A. L.; Kato, H. E.; Livingston, K. E.; Thorsen, T. S.; Kling, R. C.; Granier, S.; Gmeiner, P.; Husbands, S. M.; Traynor, J. R.; Weis, W. I.; Steyaert, J.; Dror, R. O.; Kobilka, B. K. Structural Insights into μ-Opioid Receptor Activation. *Nature* **2015**, *524*, 315–321.
(9) Manglik, A. Crystal Structure of the μ-Opioid Receptor Bound to a Morphinan Antagonist. *Nature* **2012**, *485*, 321.
(10) Koehl, A.; Hu, H.; Maeda, S.; Zhang, Y.; Qu, Q.; Paggi, J. M.; Latorraca, N. R.; Hilger, D.; Dawson, R.; Matile, H.; Schertler, G. F. X.; Granier, S.; Weis, W. I.; Dror, R. O.; Manglik, A.; Skiniotis, G.; Kobilka, B. K. Structure of the μ-Opioid Receptor-Gi Protein Complex. *Nature* **2018**, *558*, 547–552.
(11) Ballesteros, J. A.; Weinstein, H. Integrated Methods for the Construction of Three-Dimensional Models and Computational Probing of Structure-Function Relations in G Protein-Coupled Receptors. *Methods Neurosci.* **1995**, *25*, 366–428.
(12) Surrat, C. K.; Johnson, P. S.; Moriwaki, A.; Seidleck, B. K.; Blaschak, C. J.; Wang, J. B.; Uhl, G. R. Charged Transmembrane Domain Amino Acids Are Critical for Agonist Recognition And Intrinsic Activity. *J. Biol. Chem.* **1994**, *269*, 20548–20553.
(13) Mansour, A.; Taylor, L. P.; Fine, J. L.; Thompson, R. C.; Hoversten, M. T.; Mosberg, H. I.; Watson, S. J.; Akil, H. Key Residues Defining the μ-Opioid Receptor Binding Pocket: A Site-Directed Mutagenesis Study. *J. Neurochem.* **1997**, *68*, 344–353.
(14) Meyer, J.; Del Vecchio, G.; Seitz, V.; Massaly, N.; Stein, C. Modulation of M-opioid Receptor Activation by Acidic pH Is Dependent on Ligand Structure and an Ionizable Amino Acid Residue. *Br. J. Pharmacol.* **2019**, *176*, 4510–4520.
(15) Ellis, C. R.; Kruhlak, N. L.; Kim, M. T.; Hawkins, E. G.; Stavitskaya, L. Predicting Opioid Receptor Binding Affinity of Pharmacologically Unclassified Designer Substances Using Molecular Docking. *PLoS One* **2018**, *13*, e0197734.
(16) Subramanian, G.; Paterlini, M. G.; Portoghese, P. S.; Ferguson, D. M. Molecular Docking Reveals a Novel Binding Site Model for Fentanyl at the μ-Opioid Receptor. *J. Med. Chem.* **2000**, *43*, 381–391.
(17) Lipiński, P. F. J.; Jarończyk, M.; Dobrowolski, J. C.; Sadlej, J. Molecular Dynamics of Fentanyl Bound to μ-Opioid Receptor. *J. Mol. Model.* **2019**, *25*, 144.
(18) Huber, G.; Kim, S. Weighted-Ensemble Brownian Dynamics Simulations for Protein Association Reactions. *Biophys. J.* **1996**, *70*, 97–110.
(19) Zwier, M. C.; Adelman, J. L.; Kaus, J. W.; Pratt, A. J.; Wong, K. F.; Rego, N. B.; Suárez, E.; Lettieri, S.; Wang, D. W.; Grabe, M.; Zuckerman, D. M.; Chong, L. T. WESTPA: An Interoperable, Highly Scalable Software Package for Weighted Ensemble Simulation and Analysis. *J. Chem. Theory Comput.* **2015**, *11*, 800–809.
(20) Zuckerman, D. M.; Chong, L. T. Weighted Ensemble Simulation: Review of Methodology, Applications, and Software. *Annu. Rev. Biophys.* **2017**, *46*, 43–57.
(21) Wallace, J. A.; Shen, J. K. Continuous Constant pH Molecular Dynamics in Explicit Solvent with pH-Based Replica Exchange. *J. Chem. Theory Comput.* **2011**, *7*, 2617–2629.
(22) Huang, Y.; Chen, W.; Dotson, D. L.; Beckstein, O.; Shen, J. Mechanism of pH-Dependent Activation of the Sodium-Proton Antiporter NhaA. *Nat. Commun.* **2016**, *7*, 12940.
(23) Huang, Y.; Henderson, J. A.; Shen, J. Continuous constant pH Molecular Dynamics Simulations of Transmembrane Proteins. *Methods Mol. Biol.* **2020**, in press.
(24) Case, D. A.; Ben-Shalom, I. Y.; Brozell, S. R.; Cerutti, D. S.; Cheatham, T. E. I.; Cruzeiro, V. W. D.; Darden, T. A.; Duke, R. E.; Ghoreishi, D.; Gilson, M. K. AMBER 2018. 2018.
(25) Maguire, P.; Tsai, N.; Cometta-Morini, C.; Loew, G. Pharmacological Profiles of Fentanyl Analogs at Mu, Delta and Kappa Opiate Receptors. *Eur. J. Pharmacol.* **1992**, *213*, 219–225.
(26) Casy, A. F.; Huckstep, M. R. Structure-Activity Studies of Fentanyl. *J. Pharm. Pharmacol.* **1988**, *40*, 605–608.
(27) Willett, P.; Barnard, J. M.; Downs, G. M. Chemical Similarity Searching. *J. Chem. Inf. Comput. Sci.* **1998**, *38*, 983–996.
(28) Chaturvedi, K.; Shahrestanifar, M.; Howells, R. D. μ Opioid Receptor: Role for the Amino Terminus as a Determinant of Ligand Binding Affinity. *Mol. Brain Res.* **2000**, *76*, 64–72.
(29) United Nations Office on Drugs and Crime, *Fentanyl and Its Analogues – 50 Years On*; Global Smart Update, 2017.
(30) Chan, H. C. S.; Wang, J.; Palczewski, K.; Filipek, S.; Vogel, H.; Liu, Z.-J.; Yuan, S. Exploring a New Ligand Binding Site of G Protein-Coupled Receptors. *Chem. Sci.* **2018**, *9*, 6480–6489.
(31) Cong, X.; Campomanes, P.; Kless, A.; Schapitz, I.; Wagener, M.; Koch, T.; Carloni, P. Structural Determinants for the Binding of Morphinan Agonists to the μ-Opioid Receptor. *PLOS ONE* **2015**, *10*, e0135998.
(32) Schneider, S.; Provasi, D.; Filizola, M. How Oliceridine (TRV-130) Binds and Stabilizes a μ-Opioid Receptor Conformational State That Selectively Triggers G Protein Signaling Pathways. *Biochemistry* **2016**, *55*, 6456–6466.
(33) Katritch, V.; Fenalti, G.; Abola, E. E.; Roth, B. L.; Cherezov, V.; Stevens, R. C. Allosteric Sodium in Class A GPCR Signaling. *Trends Biochem. Sci.* **2014**, *39*, 233–244.
(34) Yuan, S.; Vogel, H.; Filipek, S. The Role of Water and Sodium Ions in the Activation of the μ-Opioid Receptor. *Angew. Chem. Int. Ed.* **2013**, *52*, 10112–10115.
(35) Vickery, O. N.; Carvalheda, C. A.; Zaidi, S. A.; Pisliakov, A. V.; Katritch, V.; Zachariae, U. Intracellular Transfer of Na+ in an Active-State G-Protein-Coupled Receptor. *Structure* **2018**, *26*, 171–180.e2.
(36) Alexov, E.; Mehler, E. L.; Baker, N.; Baptista, A.; Huang, Y.; Milletti, F.; Nielsen, J. E.; Farrell, D.; Carstensen, T.; Olsson, M. H. M.; Shen, J. K.; Warwicker, J.; Williams, S.; Word, J. M. PROGRESS IN THE PREDICTION OF pKa VALUES IN PROTEINS. *Proteins* **2011**, *79*, 3260–3275.
(37) Thurlkill, R. L.; Grimsley, G. R.; Scholtz, J. M.; Pace, C. N. pK values of the ionizable groups of proteins. *Protein Sci.* **2006**, *15*, 1214–1218.
(38) Brooks, B. R.; Brooks, C. L.; Mackerell, A. D.; Nilsson, L.; Petrella, R. J.; Roux, B.; Won, Y.; Archontis, G.; Bartels, C.; Boresch, S.; Caflisch, A.; Caves, L.; Cui, Q.; Dinner, A. R.; Feig, M.; Fischer, S.; Gao, J.; Hodoscek, M.; Im, W.; Kuczera, K.; Lazaridis, T.; Ma, J.; Ovchinnikov, V.; Paci, E.; Pastor, R. W.;

Post, C. B.; Pu, J. Z.; Schaefer, M.; Tidor, B.; Venable, R. M.; Woodcock, H. L.; Wu, X.; Yang, W.; York, D. M.; Karplus, M. CHARMM: The Biomolecular Simulation Program. *J. Comput. Chem.* **2009**, *30*, 1545–1614.

(39) Huang, Y.; Chen, W.; Wallace, J. A.; Shen, J. All-Atom Continuous Constant pH Molecular Dynamics With Particle Mesh Ewald and Titratable Water. *J. Chem. Theory Comput.* **2016**, *12*, 5411–5421.

(40) Zwier, M. C.; Kaus, J. W.; Chong, L. T. Efficient Explicit-Solvent Molecular Dynamics Simulations of Molecular Association Kinetics: Methane/Methane, Na+/Cl-, Methane/Benzene, and K+/18-Crown-6 Ether. *J. Chem. Theory Comput.* **2011**, *7*, 1189–1197.